Check for updates

LASER & PHOTONICS REVIEWS
www.lpr-journal.org

Topological Engineering of High-Order Exceptional Points Through Transformation Optics

Kaiyuan Wang, Qi Jie Wang, Matthew R. Foreman, and Yu Luo**

Exceptional points (EPs) in non-Hermitian photonic systems have attracted considerable research interest due to their singular eigenvalue topology and associated anomalous physical phenomena. These properties enable diverse applications ranging from enhanced quantum metrology to chiral light-matter interactions. Practical implementation of high order EPs in optical platforms however remains fundamentally challenging, requiring precise multi-parameter control that often exceeds conventional design capabilities. This work presents a novel framework for engineering high order EPs through transformation optics (TO) principles, establishing a direct correspondence between mathematical singularities and physically controllable parameters. This TO-based paradigm addresses critical limitations in conventional Hamiltonian approaches, where abstract parameter spaces lack explicit connections to experimentally accessible degrees of freedom, while simultaneously providing full mode solutions. In contrast to prevailing parity-time-symmetric architectures, this methodology eliminates symmetry constraints in EP design, significantly expanding the possibilities in non-Hermitian photonic engineering. The proposed technique enables control over EP formation and evolution in nanophotonic systems, offering new pathways for developing topological optical devices with enhanced functionality and robustness.

1. Introduction

An exceptional point (EP) is a branch point singularity that can occur in the spectrum of non-Hermitian systems. An N-th order EP (denoted henceforth as EPN) corresponds to a point in the system's parameter space at which N eigenvalues and the associated eigenstates of the non-Hermitian Hamiltonian coalesce.[1,2] EPs have been extensively studied in recent years as they can give rise to unique physical phenomena, such as unidirectional invisibility,[3,4] enhanced sensitivity,[5,6] and non-reciprocal light propagation.[7] Advances in this field have also revealed a variety of complex EP geometries in parameter space, including exceptional rings,[8,9] arcs,[10,11] surfaces,[12] and junctions,[13] which can exhibit diverse features like fractional topological charges[14,15] and an anisotropic response to external perturbations.[16,17] These properties offer significant opportunities to tailor the response of physical systems.

Nano- and micro-optical systems, including microcavities, waveguides, gratings, and nanoplasmonic structures,[18,19] have proven to be rich and flexible platforms for realizing, studying, and engineering EPs. For example, the observation of EPs in microcavity systems has enabled enhanced optical sensing capabilities,[5,20] while EPs in waveguides have facilitated the development of novel light manipulation techniques.[21,22] Current methods to design EPs in optical systems however primarily focus on the system Hamiltonian. Whilst effective in theoretical studies, the Hamiltonian approach faces significant challenges when applied to EP design in realistic physical systems. For instance, Hamiltonians considered in EP design are often limited to idealised or simplified models which do not accurately represent the complexity or

K. Wang, Q. J. Wang, M. R. Foreman
School of Electrical and Electronic Engineering
Nanyang Technological University
50 Nanyang Avenue, Singapore 639798, Singapore
E-mail: matthew.foreman@ntu.edu.sg

The ORCID identification number(s) for the author(s) of this article can be found under https://doi.org/10.1002/lpor.202500593

© 2025 The Author(s). Laser & Photonics Reviews published by Wiley-VCH GmbH. This is an open access article under the terms of the Creative Commons Attribution-NonCommercial License, which permits use, distribution and reproduction in any medium, provided the original work is properly cited and is not used for commercial purposes.

DOI: 10.1002/lpor.202500593

K. Wang, M. R. Foreman
Institute for Digital Molecular Analytics and Science
59 Nanyang Drive, Singapore 636921, Singapore

Q. J. Wang
Centre for Disruptive Photonic Technologies
School of Physical and Mathematical Sciences
Nanyang Technological University
Singapore 637371, Singapore

Y. Luo
National Key Laboratory of Microwave Photonics
Nanjing University of Aeronautics and Astronautics
Nanjing 211106, China
E-mail: yu.luo@nuaa.edu.cn

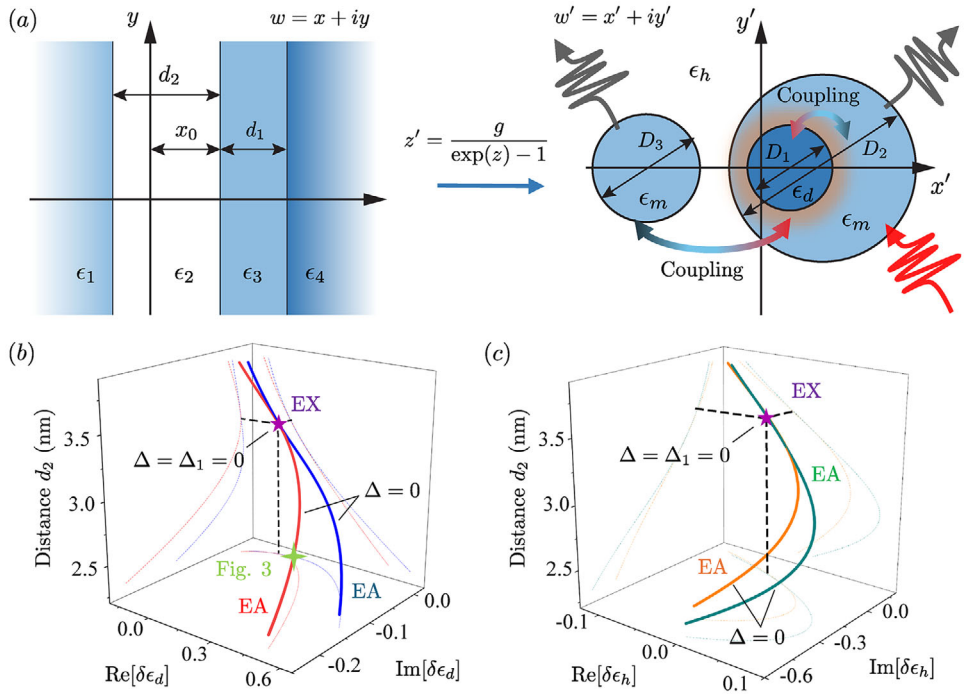

Figure 1. TO approach to designing exceptional points. a) Schematic diagram of planar geometry considered before (left) and plasmonic nanowire geometry consider after (right) transformation. b) Exceptional arcs (EA) of exceptional points (EPs), defined by $\Delta = 0$ (see main text), traced in physical parameter space upon variation of the electric permittivity of gain material and interface separation d_2. The intersection of the two EAs corresponds to an exceptional nexus (EX), a point at which a higher order EP exists. c) As (b) albeit for variations in host material.

capture intricate interactions present in practical systems, especially at the nanoscale. Such issues are further compounded in the design of high order exceptional points, which requires precise adjustment of $2N-2$ real parameters in general, which is challenging in practice.[22,23] Although specific symmetries, such as pseudo-Hermitian, or chiral symmetry, can help reduce the difficulty of finding EPs,[24,25] generalizing these symmetries to the generation of higher-order EPs remains an open problem.[26,27]

In this work, we propose an approach to design high order EPs which leverages transformation optics (TO) and is capable of alleviating limitations of the Hamiltonian based approach. TO is a powerful and versatile method that allows manipulation of electromagnetic fields through engineering material properties.[28] The flexibility of TO allows us to not only model complex geometries but also to design EPs with specific mode distributions. Our approach moreover does not rely on PT symmetry, thereby enabling the design of non-PT symmetric EPs, which have garnered significant attention due to their broader range of unique properties.[19,29–31]

2. Design principles and results

Transformation optics exploits the invariance of Maxwell's equations under coordinate transformations, such that known electromagnetic solutions for simple geometries can be mapped to more complex structures.[32,33] By first deriving the canonical resonance condition for modes in a planar multilayered structure, we can conveniently tailor the physical parameters of the system to generate high order EPs, before the solution is finally mapped to a more complicated geometry. In this work we focus on design of EPs in nanoplasmonic systems. Noting that in a multilayer geometry, each interface can potentially support a surface plasmon polariton (SPP) mode, an Nth order EP can thus in principle be designed for a system with N interfaces ($N+1$ layers).[22] Existence of an Nth order EP, however, requires that the resonance equation be expressible as an Nth order polynomial in one of the frequency dependent system parameters (typically electric permittivity), and that this polynomial possesses N repeated roots. These constraints help guide system design and allow us to determine suitable material and geometric parameters to realise high order EPs.

For concreteness, we illustrate the approach through construction and analysis of a third-order EP in a coupled core-shell/monomer nanowire system as depicted in **Figure 1a**. We therefore begin by considering a general 2D four layer system, with electric permittivities ϵ_j for integer $j \in [1,4]$ and interface separations d_1 and d_2 as shown in Figure 1a. In the quasi-static limit, we can express supported modes in terms of their scalar potential distribution, from which we can derive the corresponding electric and displacement fields, $\mathbf{E}$ and $\mathbf{D}$ respectively (see the Supplementary Material for further details and alternative derivations). Application of standard boundary conditions for the tangential (normal) components of the electric (displacement) field at each interface yields a set of linear equations relating the tangential electric field component at each interface, specifically

$$\mathbb{M}^{(3)}\mathbf{E}^{(3)} = \mathbf{0} \tag{1}$$

© 2025 The Author(s). Laser & Photonics Reviews published by Wiley-VCH GmbH

18638899, 2026, 3, Downloaded from https://onlinelibrary.wiley.com/doi/10.1002/lpor.202500593, Wiley Online Library on [02/11/2026]. See the Terms and Conditions (https://onlinelibrary.wiley.com/terms-and-conditions) on Wiley Online Library for rules of use; OA articles are governed by the applicable Creative Commons License

where

$$\mathbb{M}^{(3)} = \begin{bmatrix} \mathcal{M}(d_2, \epsilon_2, \epsilon_1) & -\epsilon_2 & 0 \\ 0 & -\epsilon_3 & \mathcal{M}(d_1, \epsilon_3, \epsilon_4) \\ \mathcal{M}(d_2, \epsilon_1, \epsilon_2) & 0 & \mathcal{M}(d_1, \epsilon_4, \epsilon_3) \end{bmatrix}, \tag{2}$$

$$\mathbf{E}^{(3)} = \begin{bmatrix} E_y(x_0 - d_2) \\ E_y(x_0) \\ E_y(x_0 + d_1) \end{bmatrix}, \tag{3}$$

$\mathcal{M}(d, \epsilon_a, \epsilon_b) = \epsilon_a \cosh(|k|d) + \epsilon_b \sinh(|k|d)$ and k is the tangential wavenumber along the interface. Resonances correspond to non-trival solutions of Equation (1) which occur when

$$\det[\mathbb{M}^{(3)}] = \epsilon_2 \mathcal{M}(d_1, \epsilon_3, \epsilon_4)\mathcal{M}(d_2, \epsilon_1, \epsilon_2) + \epsilon_3 \mathcal{M}(d_1, \epsilon_4, \epsilon_3)\mathcal{M}(d_2, \epsilon_2, \epsilon_2) = 0. \tag{4}$$

Equation (4) in its most general form is quadratic in the permittivity of any given layer and therefore it is not readily apparent how to design EPs of order higher than 2. By asserting, however, that two layers have identical permittivity (whilst keeping the number of interfaces fixed), Equation (4) can be expressed as a cubic equation. Specifically, if we assume $\epsilon_1 = \epsilon_3 = \epsilon_m$ (which we take as a lossy metal in what follows), $\epsilon_2 = \epsilon_h$ (a "host" dielectric material) and $\epsilon_4 = \epsilon_d$ (dielectric), Equation (4) can be written as

$$A\epsilon_m^3 + B\epsilon_m^2 + C\epsilon_m + D = 0, \tag{5}$$

where the coefficients are defined in the Supporting Information. Notably, these material choices do not correspond to a PT symmetric system. Furthermore, note that Equation (5) can be considered as the characteristic equation of some eigenvalue problem $|\mathbb{A} - \epsilon_m \mathbb{I}| = 0$, such that we will refer to values of ϵ_m satisfying Equation (5) (denoted $\epsilon_{m,r}$ for $r = 1, 2, 3$) as eigenvalues. The corresponding frequencies ω_r for which $\epsilon_m(\omega_r) = \epsilon_{m,r}$ shall be termed resonant eigenfrequencies. To generate a third order degeneracy we apply the well known criteria for a cubic equation to have three repeated roots. Specifically, letting the discriminant $\Delta = (4\Delta_1^3 - \Delta_2^2)/(27A^2)$, where $\Delta_1 = B^2 - 3AC$ and $\Delta_2 = 2B^3 - 9ABC + 27A^2D$,[34] we require $\Delta = \Delta_1 = 0$. For our example, the repeated root is then given by

$$\epsilon_m = -\frac{B}{3A} = -\frac{1}{3}\left(\epsilon_h[1 + \coth(kd_1)]\coth(kd_2) + \epsilon_d \coth(kd_1)\right). \tag{6}$$

Noting that the metal is lossy and that k, d_1 and d_2 are real positive numbers, Equation (6) implies that either ϵ_h or ϵ_d (or both) must have an imaginary part of opposite sign to ϵ_m, i.e., must possess gain. Henceforth, we consider the case $\mathrm{Im}[\epsilon_h] = 0$ and that ϵ_d describes a material with gain, as depicted in Figure 1a. According to the principles of TO, the same conditions also govern the mode spectrum in the coupled nanowire geometry shown on the right of Figure 1a, which can be generated through application of the exponential conformal mapping:[35]

$$w' = \frac{g}{\exp(w) - 1} \tag{7}$$

where $w^{(\prime)} = x^{(\prime)} + iy^{(\prime)}$, (x, y) are the untransformed spatial coordinates and primes denote transformed quantities. The parameter g is a scaling constant that controls the diameter of the nanowires (D_1, D_2, D_3 defined in the Supplement) in the transformed geometry. We assume that g is chosen such that the dimensions of the nanowire system are smaller than the optical wavelength, whereby the quasi-static model holds. Within this limit, the change in permeability after transformation can also be ignored.[36] Finally, we note, that the periodicity of the transformation implies $k = n$ ($n \in \mathbb{Z}$), which physically corresponds to the angular momentum of the corresponding mode.

For material and geometric parameters satisfying $\Delta = \Delta_1 = 0$ and Equation (6), the solutions of Equation (4) are threefold degenerate. Accordingly, these equations describe necessary parameteric constraints which must be fulfilled to realise an EP3 and hence provides direct physical insight into the design of high order EPs. For example, assuming a fixed host material (here taken as water with $\epsilon_h = 1.76$), and interface seperation d_1 the constraints $\Delta = \Delta_1 = 0$ allow us to select appropriate dielectric materials (and corresponding required levels of gain) and nanowire radii, such that Equation (6) dictates the necessary metal permittivity to generate a third order degenerate point. Using known metallic dispersion equations (taken here as the Drude-Sommerfeld model with $\epsilon_\infty = 5$, $\omega_p = 8.9$ eV, $\Gamma = 18$ fs corresponding to silver,[37]) the degenerate eigenfrequency can then be found. Assuming, $d_1 = 0.84$, $x_0 = 0.1$ and $m = 1$, we find from the repeated root constraints that $d_2 = 2$ (yielding $D_1 = 199$ nm, $D_2 = 18$ nm and $D_3 = 6$ nm for $g = 2 \times 10^{-8}$). Equation (6) then yields $\epsilon_m = (-1.548 + 0.856i)$ corresponding to a third order degeneracy at $\omega_{EP} = (8.352 + 0.250i) \times 10^{14}$ Hz. We neglect non-local effects in the material permittivities for simplicity.[38,39]

To verify the degeneracy of the modes predicted using the TO approach and its exceptional nature, we analyze the properties of the nanowire system in the vicinity of the expected EP3. In **Figure 2a** we present a plot of the logarithm of the scattering cross-section calculated as a function of gain and frequency using the method described in Ref. [40]. Selected line profiles (denoted *I–V*) are also shown in Figure 2(b), in which evolution of individual spectral peaks with material gain is illustrated. At low gains (line profile I and II), three spectral peaks are evident, which merge into a single broad peak at the EP3 (line profile III) before splitting again as gain is increased further (line profile IV and V). Accompanying blue data markers in Figure 2b, found via rigorous finite element COMSOL simulations, show good agreement with the theoretical TO based calculations. Specifically, the average relative error and its standard deviation across the frequency range shown are 5.5% and 0.17% respectively. Solid coloured lines in Figure 2a represent the real part of the eigenfrequencies, i.e., $\mathrm{Re}[\omega_r]$, calculated via numerical solution of Equation (5). In general three distinct modes are found, however at the predicted EP the real part of the eigenfrequencies clearly coalesce. The inset in the lower right of Figure 2a shows the corresponding coalles-

© 2025 The Author(s). Laser & Photonics Reviews published by Wiley-VCH GmbH

18638899, 2026, 3, Downloaded from https://onlinelibrary.wiley.com/doi/10.1002/lpor.202500593, Wiley Online Library on [02/11/2026]. See the Terms and Conditions (https://onlinelibrary.wiley.com/terms-and-conditions) on Wiley Online Library for rules of use; OA articles are governed by the applicable Creative Commons License

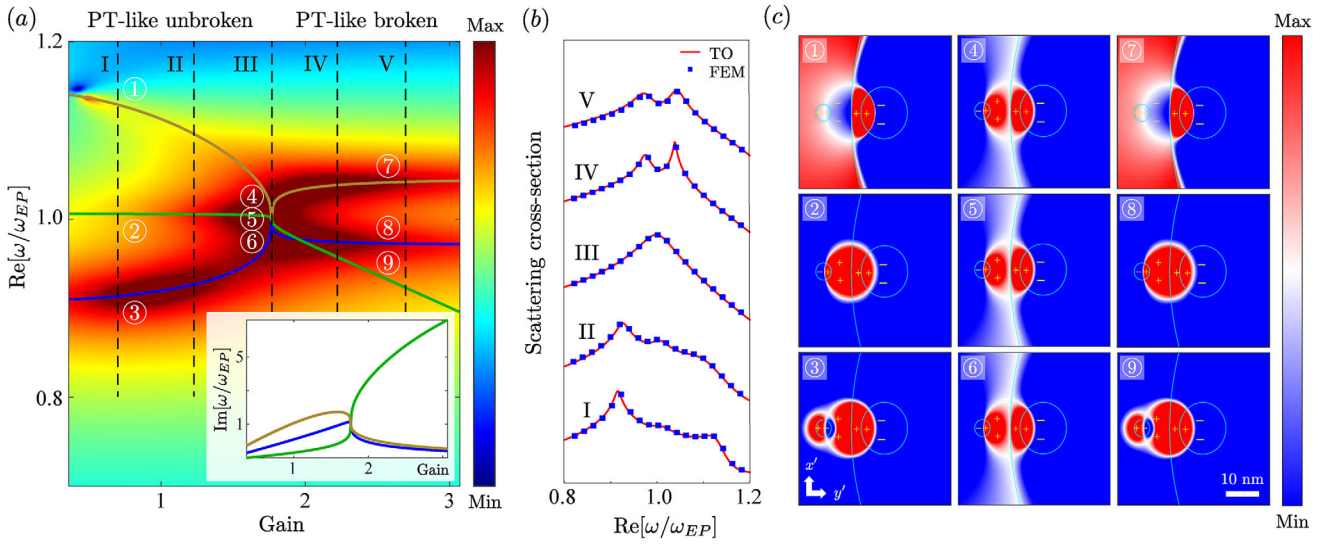

Figure 2. EP3 in core-shell/monomer coupled nanowire system. a) Color density plot of the logarithm of the scattering cross-section of the coupled core-shell and monomer structures as a function of gain and frequency. Solid lines represent the real parts of the three eigenfrequencies (corresponding imaginary parts are shown in the inset). b) Scattering cross-sections corresponding to *I–V* in (a) as found using our TO approach (red lines) and finite element simulations (blue markers). c) Potential distributions for eigenmodes at points labelled ①-⑨ in (a). The + and − markers denote a positive and negative potential respectively. Cyan lines demark the nanowire interfaces (only a small part of core-shell nanowire in vicinity of monomer is shown to enhance visibility). Panels ④-⑥ correspond to the EP3.

ence of the imaginary part of the eigenfrequency and illustrates the significant changes in loss associated with the emergence of the EP.[41] Specifically, in the PT-like unbroken phase, the mode corresponding to the green line exhibits relatively low loss, whereas in the PT-like broken phase, the loss increases sharply resulting in relatively weak scattering. In contrast, the loss for the other modes (blue and brown lines), decreases with increasing gain in the PT-like broken phase. This strong difference in loss means that at higher gains, only the two low loss spectral peaks are visible in the scattering spectrum (line profiles IV and V).

Degeneracy in the complex eigenfrequencies, whilst suggestive, does not unequivocally demonstrate that solutions to Equation (5) correspond to an EP. To demonstrate that the found degenerate point is indeed an EP3, we also show that the mode distributions for each eigenfrequency are identical at the degenerate point. Our TO method can fortunately provide direct information about the potential distributions for each plasmonic mode, which is often beyond the reach of traditional Hamiltonian approaches without additional modelling. Specifically, through Gaussian elimination it is simple to show that the solutions to Equation (1) take the form (with our material assumptions)

$$\begin{bmatrix} E_y(x_0 - d_2) \\ E_y(x_0) \\ E_y(x_0 + d_1) \end{bmatrix} = \begin{bmatrix} 1 \\ \epsilon_h^{-1}\mathcal{M}(d_2, \epsilon_h, \epsilon_m) \\ \frac{\epsilon_m \mathcal{M}(d_2,\epsilon_h,\epsilon_m)}{\epsilon_h \mathcal{M}(d_2,\epsilon_m,\epsilon_d)} \end{bmatrix}, \tag{8}$$

from which the full potential distributions follow. Example distributions are shown in Figure 2(c) for the points ①-⑨ on the resonance branches indicated in Figure 2a. Color scales for each diagram span the respective maximum and minimum potential and are not necessarily the same for each panel. For non-degenerate conditions (①-③ and ⑦-⑨) the nanowire structure exhibits standard plasmonic modes, including symmetric and asymmetric distributions at different boundaries. In contrast, at the degenerate point, the modes found for each branch are identical (④-⑥) as expected for an EP. Moreover, the distributions are highly confined and exhibit unique spatial distributions not observed in lower order EPs. These patterns thus highlight the complexity and richness of the physical phenomena occurring at higher-order EPs.

Relaxing our previous constraint that $\Delta_1 = 0$, whilst still requiring that the discriminant of Equation (5) be zero ($\Delta = 0$), implies that Equation (5) possesses only two repeated roots.[34] We find that $\Delta = 0$ therefore defines curves in parameter space corresponding to systems supporting second (lower) order EPs. To illustrate this point we introduce perturbations $\delta\epsilon_h$ and $\delta\epsilon_d$, corresponding to variations in the complex electric permittivity of the host and dielectric gain material respectively, away from the EP3. Figure 1b shows the resulting EP2 exceptional arcs (EA)[10,11] in the $(d_2, \delta\epsilon_h)$ domain when $\delta\epsilon_d = 0$. Similarly, Figure 1c illustrates the case for perturbations in the gain material ($\delta\epsilon_d \neq 0$, $\delta\epsilon_h = 0$). Note that in each case two arcs result since Δ is quadratic in the corresponding system parameters. Through our TO analysis we can therefore easily determine the family of coupled nanowire configurations supporting EP2s, and how to tune particular parameters (such as wire radius) to move along these EAs to reach the point of convergence, i.e., the exceptional nexus (EX), and generate the resulting higher order EP3. We note that this insight and practical tunability is typically absent from Hermitian based design philosophies which consider more abstracted perturbations, e.g., to modal coupling constants, in contrast to the real physically relevant perturbations considered in our model. **Figure** 3a analyzes the EP2 at a position along the exceptional EA, in a manner similar to Figure 2. We first note that, as shown in Figure 3a, the eigenfrequencies corresponding to the brown

© 2025 The Author(s). Laser & Photonics Reviews published by Wiley-VCH GmbH

18638899, 2026, 3, Downloaded from https://onlinelibrary.wiley.com/doi/10.1002/lpor.202500593, Wiley Online Library on [02/11/2026]. See the Terms and Conditions (https://onlinelibrary.wiley.com/terms-and-conditions) on Wiley Online Library for rules of use; OA articles are governed by the applicable Creative Commons License

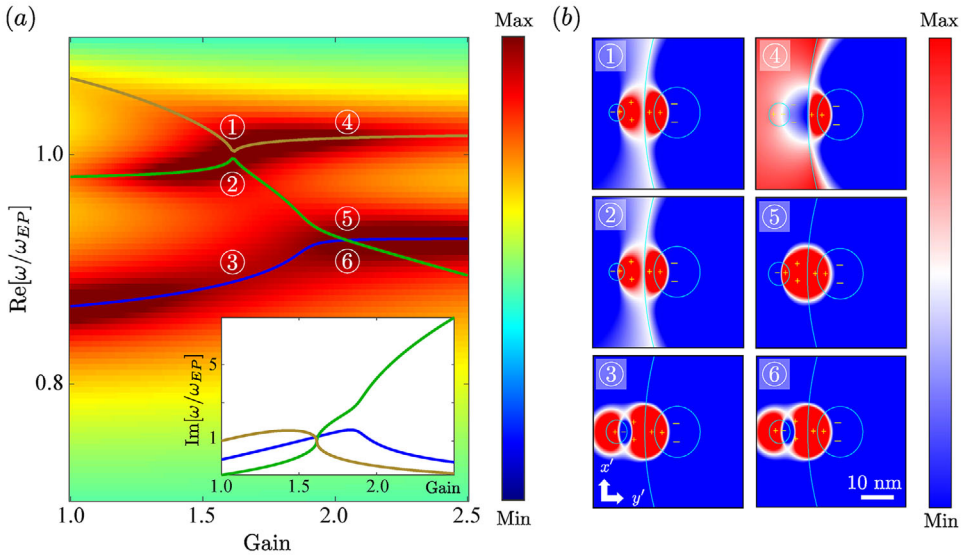

Figure 3. EP2 in core-shell/monomer coupled nanowire system. a) As Figure 2a albeit for system parameters lying on the EA away from the EX (see Figure 1). b) Potential distributions for ①-⑥ in (a), in which + and − denote a positive and negative potential respectively. Panels ⑤ and ⑥correspond to the crossing of the real part of the eigenfrequecies, whereas the identical distributions in ① and ② signify an EP2.

and green solid lines possess the same real and imaginary parts for gains ∼ 1.6, indicating the presence of an EP2, which is confirmed by the degenerate mode distributions shown in panels ⑤ and ⑥ of Figure 3b. It is interesting, to note that at a gain of ∼ 2, the real parts of the eigenfrequencies traced by the blue and green curves are equal, however their imaginary parts (inset of Figure 3a) remain different demonstrating this point is not a true degeneracy.[42]

To further demonstrate the capabilities and versatility of our method in designing higher-order EPs, we have explored two further scenerios. First, we consider design of EPs with different angular momenta, n. The corresponding potential distributions found for third order EPs in a core-shell/monomer nanowire system with angular momenta of $n = 2$, $n = 3$ and $n = 4$ are shown in **Figure** 4.

Second, we consider design of a fourth-order exceptional point (EP4). Specifically, by considering a 5 layer gain-loss multilayer structure distributed symmetrically around the y-axis, we can generate, through application of Equation (7), a PT symmetric configuration of two adjacent core-shell structured nanowires. The metallic outer shell of one nanowire is assumed to be described by electric permittivity $\epsilon_m = \epsilon_\infty - \omega_p^2/\omega^2 + i\alpha$, whereas the inner dieletric core has $\epsilon_d = \epsilon - i\beta$, where α and β are frequency independent parameters, $\epsilon = 1.84$, $\epsilon_\infty = 5$ and $\omega_p = 8.9$ eV. PT symmetry therefore implies for the other nanowire the core and shell have permittivities ϵ_m^* and ϵ_d^* respectively. The host material is taken to be air with unity permittivity. **Figure** 5a shows the resulting distribution of the logarithmic scattering cross-section as a function of ϵ and frequency. Using the assumed analytic forms of the permittivity functions, the resonance condition can be expressed as a polynomial in frequency ω, specifically, $A\omega^8 + B\omega^6 + C\omega^4 + D\omega^2 + E = 0$, which is quartic in ω^2 with three distinct roots. As before, the curves in Figure 5a represent the real part of the eigenfrequencies, Re[ω_r], found from the corresponding resonance condition (see Supplementary Material). To aid visibility of overlapping branches, some curves are plotted using a dashed line style. The inset to Figure 5a shows the corresponding imaginary part of the eigenfrequencies as a function of relative permittivity, which exhibit significantly different behaviour between the PT-unbroken and broken phases. Symmetry in the core-shell structures also leads to the existence of dark modes, resulting in weak scattering (and low scattering cross-sections) in spite of small modal losses.[43,44] The mode distributions can again be found (see Supporting Information) and are shown at assorted positions along the resonance branches in Figure 5c as marked ①-⑨ in Figure 5a. Constraints for the existence of multiple repeated roots (2, 3, or 4) are known[34] and can therefore be used to design exceptional points of higher order. In our case we seek an EP4 and use the constraints $8AC - 3B^2 = B^3 - 4ABC + 8A^2D = 16AB^2C - 64A^2BD - 3B^4 + 256A^3E = 0$, which yields an EP4 at position ⑤ in parameter space. The good agreement between TO based predictions and rigorous COMSOL simulation results for the scattering cross-section, shown in Figure 5, validates our approach. Specifically, the absolute relative error was calculated to

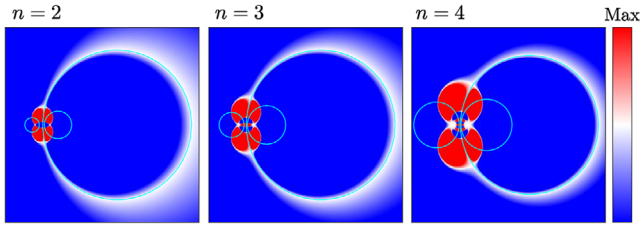

Figure 4. EP3s with different angular momenta. Potential distributions for modes with angular momenta (left) $n = 2$, (middle) $n = 3$ and (right) $n = 4$, evaluated at an EP3 in a system analagous to that shown in Figure 2.

© 2025 The Author(s). Laser & Photonics Reviews published by Wiley-VCH GmbH

18638899, 2026, 3, Downloaded from https://onlinelibrary.wiley.com/doi/10.1002/lpor.202500593, Wiley Online Library on [02/11/2026]. See the Terms and Conditions (https://onlinelibrary.wiley.com/terms-and-conditions) on Wiley Online Library for rules of use; OA articles are governed by the applicable Creative Commons License

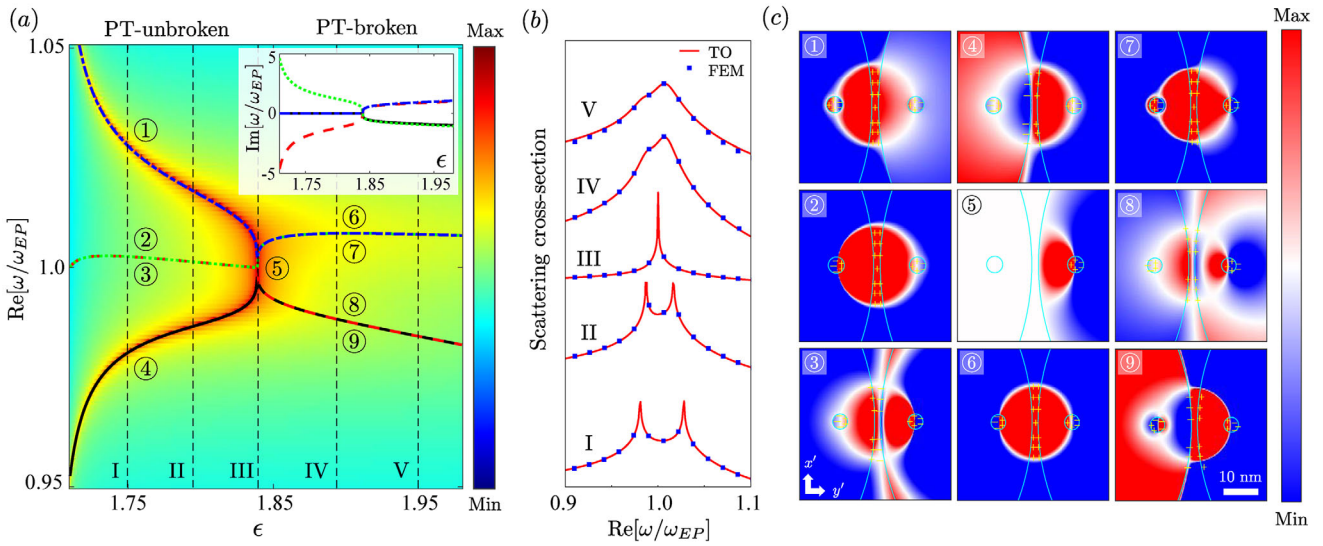

Figure 5. EP4 in core-shell dimer nanowire system. a) Color density plot of the logarithm of the scattering cross-section of the coupled core-shell dimer structure as a function of ϵ and frequency. Solid and dashed lines represent the real parts of the four eigenfrequencies (corresponding imaginary parts are shown in the inset). b) Scattering cross-sections corresponding to I-V in (a) as found using our TO approach (red lines) and finite element simulations (blue markers). c) Potential distributions for eigenmodes at points labelled ①-⑨ in (a). The + and − markers denote a positive and negative potential respectively. Cyan lines demark the nanowire interfaces (only a small part of core-shell nanowires are shown to enhance visibility). Panel ⑤ corresponds to the EP3.

have a mean of ∼ 0.54% and a standard deviation of ∼ 0.16%. Agreement between analytic and simulated mode distributions was also found.

3. Conclusion

This work has introduced a novel TO based approach for designing high-order EPs in nanoplasmonic systems. By utilising TO, we have mapped solutions from simple multilayer geometries to complex nanowire structures, enabling the design of EPs with targeted properties. Specifically, we have demonstrated the realization of an EP3 in a coupled core-shell/monomer nanowire system, identifying the precise constraints on system parameters required to achieve the desired degeneracy. Finite element simulations were used to confirm the existence and exceptional nature of the EP3. Furthermore, we have shown how this approach can be extended to design EP2s along exceptional arcs, revealing a pathway to higher-order EPs through parameter space manipulation. The versatility of our method was further highlighted by the demonstration of EP3s with varying angular momenta and the design of a EP4 in a coupled core-shell dimer system. Our TO-based methodology overcomes limitations of traditional Hamiltonian approaches, which often struggle to connect abstract model parameters to experimentally controllable variables. Moreover, our approach naturally yields corresponding mode distributions without requiring additional modelling. Accordingly, the TO methodology offers a powerful and flexible framework for engineering EPs in complex non-Hermitian nanophotonic structures. Experimentally, introducing moderate optical gain adjacent to metals, e.g., through use of dyes, fluorescent polymers or quantum dots, has been shown to enable compensation of plasmonic losses and nanoscale lasing,[45–48] thereby supporting the practicality of the gain-assisted exceptional points considered here. Our work therefore opens new avenues for applications in sensing, light manipulation, and other areas where precise control over light-matter interaction is crucial.

Supporting Information

Supporting Information is available from the Wiley Online Library or from the author.

Acknowledgements

K.W. was funded by an Interdisciplinary Graduate Programme PhD Research Scholarship through the Institute for Digital Molecular Analytics and Science (IDMxS) under the Singapore Ministry of Education Research Centres of Excellence scheme (EDUN C-33-18-279-V12). M.R.F. acknowledges further funding from Singapore Ministry of Education Academic Research Fund (Tier 1) Grant No. RS13/23. Y.L. acknowledges funding support from Fundamental Research Funds for the Central Universities, NUAA (No. NE2024007).

Conflict of Interest

The authors declare no conflict of interest.

Data Availability Statement

The data that support the findings of this study are available from the corresponding author upon reasonable request.

Keywords

exceptional points, nanoplasmonics, non-Hermitian physics, transformation optics

© 2025 The Author(s). Laser & Photonics Reviews published by Wiley-VCH GmbH

18638899, 2026, 3, Downloaded from https://onlinelibrary.wiley.com/doi/10.1002/lpor.202500593, Wiley Online Library on [02/11/2026]. See the Terms and Conditions (https://onlinelibrary.wiley.com/terms-and-conditions) on Wiley Online Library for rules of use; OA articles are governed by the applicable Creative Commons License

Received: March 16, 2025
Revised: September 6, 2025
Published online: September 30, 2025

[1] M.-A. Miri, A. Alú, *Science* **2019**, *363*, eaar7709.
[2] W. D. Heiss, *J. Phys. A: Math. Theor.* **2012**, *45*, 444016.
[3] L. Feng, Z. J. Wong, R.-M. Ma, Y. Wang, X. Zhang, *Science* **2013**, *346*, 972.
[4] A. Regensburger, C. Bersch, M.-A. Miri, G. Onishchukov, D. N. Christodoulides, U. Peschel, *Nature* **2012**, *488*, 167.
[5] W. Chen, Ş. K. Özdemir, G. Zhao, J. Wiersig, L. Yang, *Nature* **2017**, *548*, 192.
[6] H. Loughlin, V. Sudhir, *Phys. Rev. Lett.* **2024**, *132*, 243601.
[7] B. Peng, Ş. K. Özdemir, F. Lei, F. Monifi, M. Gianfreda, G. L. Long, S. Fan, F. Nori, C. M. Bender, L. Yang, *Nat. Phys.* **2014**, *10*, 394.
[8] B. Zhen, C. W. Hsu, Y. Igarashi, L. Lu, I. Kaminer, A. Pick, S.-L. Chua, J. D. Joannopoulos, M. Soljačić, *Nature* **2015**, *525*, 354.
[9] A. Cerjan, S. Huang, K. P. Chen, Y. D. Chong, M. C. Rechtsman, *Nat. Photonics* **2019**, *13*, 623.
[10] H. Shen, B. Zhen, L. Fu, *Phys. Rev. Lett.* **2018**, *120*, 146402.
[11] H. Zhou, C. Peng, Y. Yoon, C. W. Hsu, K. A. Nelson, L. Fu, J. D. Joannopoulos, M. Soljačić, B. Zhen, *Science* **2018**, *359*, 1009.
[12] Q. Zhong, J. Ren, M. Khajavikhan, D. N. Christodoulides, R. El-Ganainy, *Phys. Rev. Lett.* **2019**, *122*, 153902.
[13] E. J. Bergholtz, J. C. Budich, *Phys. Rev. Res.* **2019**, *1*, 012003.
[14] F. Song, S. Yao, Z. Wang, *Phys. Rev. Lett.* **2019**, *123*, 170401.
[15] A. Cerjan, M. Xiao, L. Yuan, S. Fan, *Phys. Rev. B* **2018**, *97*, 075128.
[16] L. Pan, S. Chen, X. Cui, *Phys. Rev. A* **2019**, *99*, 011601.
[17] E. J. Bergholtz, J. C. Budich, F. K. Kunst, *Rev. Mod. Phys.* **2021**, *93*, 015005.
[18] Z. Yang, B. Zhang, *Adv. Opt. Mater.* **2020**, *8*, 1901533.
[19] R. E. Ganainy, K. G. Makris, M. Khajavikhan, Z. H. Musslimani, S. Rotter, D. N. Christodoulides, *Nat. Phys.* **2018**, *14*, 11.
[20] H. Hodaei, A. U. Hassan, S. Wittek, H. Garcia-Gracia, R. El-Ganainy, D. N. Christodoulides, M. Khajavikhan, *Nature* **2017**, *548*, 187.
[21] J. Doppler, A. A. Mailybaev, J. Böhm, U. Kuhl, A. Girschik, F. Libisch, T. J. Milburn, P. Rabl, N. Moiseyev, S. Rotter, *Nature* **2016**, *537*, 76.
[22] I. Mandal, E. J. Bergholtz, *Phys. Rev. Lett.* **2021**, *127*, 186601.
[23] K. Ding, C. Fang, G. Ma, *Nat. Rev. Phys.* **2022**, *4*, 745.
[24] S. Sayyad, F. K. Kunst, *Phys. Rev. Res.* **2022**, *4*, 023130.
[25] A. Montag, F. K. Kunst, *Phys. Rev. Res.* **2024**, *6*, 023205.
[26] A. U. Hassan, H. Hodaei, M.-A. Miri, M. Khajavikhan, D. N. Christodoulides, *Phys. Rev. A* **2015**, *92*, 063807.
[27] Y. Liu, X. Zhang, *Nanoscale* **2012**, *4*, 5277.
[28] H. Chen, C. T. Chan, P. Sheng, *Nat. Mater.* **2010**, *9*, 387.
[29] K. G. Makris, R. El-Ganainy, D. N. Christodoulides, Z. H. Musslimani, *Phys. Rev. Lett.* **2008**, *100*, 103904.
[30] M. McCall, J. B. Pendry, V. Galdi, Y. Lai, S. A. R. Horsley, J. Li, J. Zhu, R. C. Mitchell-Thomas, O. Quevedo-Teruel, P. Tassin, V. Ginis, E. Martini, G. Minatti, S. Maci, M. Ebrahimpouri, Y. Hao, P. Kinsler, J. Gratus, J. M. Lukens, A. M. Weiner, U. Leonhardt, I. I. Smolyaninov, V. N. Smolyaninova, R. T. Thompson, M. Wegener, M. Kadic, S. A. Cummer, *J. Opt.* **2018**, *20*, 063001.
[31] F. Sun, B. Zheng, H. Chen, W. Jiang, S. Guo, Y. Liu, Y. Ma, S. He, *Laser Photonics Rev.* **2017**, *11*, 1700034.
[32] N. B. Kundtz, D. R. Smith, J. B. Pendry, *Proc. IEEE* **2010**, *99*, 1622.
[33] J. B. Pendry, D. Schurig, D. R. Smith, *Science* **2006**, *312*, 1780.
[34] S. Neumark, Solution of Cubic and Quartic Equations, Elsevier, **2014**.
[35] A. Aubry, D. Y. Lei, S. A. Maier, J. B. Pendry, *ACS Nano* **2011**, *5*, 3293.
[36] J. B. Pendry, A. I. Fernández-Domínguez, Y. Luo, R. Zhao, *Nat. Phys.* **2013**, *9*, 518.
[37] H. U. Yang, J. D'Archangel, M. L. Sundheimer, E. Tucker, G. D. Boreman, M. B. Raschke, *Phys. Rev. B* **2015**, *91*, 235137.
[38] F. J. G. de Abajo, *J. Phys. Chem. C* **2008**, *112*, 17983.
[39] K. J. Savage, M. M. Hawkeye, R. Esteban, A. G. Borisov, J. Aizpurua, J. J. Baumberg, *Nature* **2012**, *491*, 574.
[40] A. Aubry, D. Y. Lei, S. A. Maier, J. B. Pendry, *Phys. Rev. B* **2010**, *82*, 205109.
[41] K. Wang, L. Xiao, H. Lin, W. Yi, E. J. Bergholtz, P. Xue, *Sci. Adv.* **2023**, *9*, eadi0732.
[42] H. Z. Chen, , T. Liu, , H. Y. Luan, , R. J. Liu, , X. Y. Wang, , X. F. Zhu, , Y. B. Li, , Z. M. Gu, , S. J. Liang, , H. Gao, , L. Lu, , L. Ge, , S. Zhang, , J. Zhu, , R. M. Ma, *Nat. Phys.* **2020**, *16*, 571.
[43] Y. Gao, N. Zhou, Z. Shi, X. Guo, L. Tong, *Photonics Research* **2018**, *6*, 887.
[44] D. E. Gómez, Z. Q. Teo, M. Altissimo, T. J. Davis, S. Earl, A. Roberts, *Nano Lett.* **2013**, *13*, 3722.
[45] I. De Leon, P. Berini, *Nat. Photonics* **2010**, *4*, 382.
[46] R. F. Oulton, V. J. Sorger, T. Zentgraf, R.-M. Ma, C. Gladden, L. Dai, G. Bartal, X. Zhang, *Nature* **2009**, *461*, 629.
[47] M. C. Gather, K. Meerholz, N. Danz, K. Leosson, *Nat. Photonics* **2010**, *4*, 457.
[48] S. J. P. Kress, F. Vogelbacher, P. Heuser, S. Jungclaus, A. Tittl, S. Lerch, R. Hillenbrand, M. Klar, T. A. F. König, H. Giessen, *Sci. Adv.* **2017**, *3*, e1501802.

© 2025 The Author(s). Laser & Photonics Reviews published by Wiley-VCH GmbH

18638899, 2026, 3, Downloaded from https://onlinelibrary.wiley.com/doi/10.1002/lpor.202500593, Wiley Online Library on [02/11/2026]. See the Terms and Conditions (https://onlinelibrary.wiley.com/terms-and-conditions) on Wiley Online Library for rules of use; OA articles are governed by the applicable Creative Commons License